J. Phys. B: At. Mol. Opt. Phys. **41** (2008) 215506 (7pp) doi:10.1088/0953-4075/41/21/215506

Storing quantum states in bosonic dissipative networks

M A de Ponte[1], S S Mizrahi[1] and M H Y Moussa[2]

[1] Departamento de Física, Universidade Federal de São Carlos, Caixa Postal 676, São Carlos, 13565-905, São Paulo, Brazil
[2] Instituto de Física de São Carlos, Universidade de São Paulo, Caixa Postal 369, 13560-590 São Carlos, SP, Brazil

Received 6 August 2008
Published 23 October 2008
Online at stacks.iop.org/JPhysB/41/215506

Abstract
By considering a network of dissipative quantum harmonic oscillators, we deduce and analyse the optimum topologies which are able to store quantum superposition states, protecting them from decoherence, for the longest period of time. The storage is made dynamically, in that the states to be protected evolve through the network before being retrieved back in the oscillator where they were prepared. The decoherence time during the dynamic storage process is computed and we demonstrate that it is proportional to the number of oscillators in the network for a particular regime of parameters.

1. Introduction

In recent years the focus on subjects such as quantum state transfer [1–4], entanglement distribution [5] and decoherence [6–8] in quantum networks has indicated an irreversible trend in information theory towards many-body physics. This is corroborated by the recently revealed scaling of entanglement due to the many-body effects of phase transitions [9], superradiance [10] and superconductivity [11]. In fact, the path of information theory towards many-body physics is naturally imposed by the prospect of achieving scalable quantum processors [12].

In the specific subject of state transfer in quantum networks, a great deal of work has been conducted in many different systems. The coherent transport of atomic wave packets [1] and the evolution of macroscopically entangled states [2] have been analysed within optical lattices. The perfect transfer of arbitrary states has been proposed theoretically in quantum spin networks [3]. In the quantum optics domain, coherent quantum state transfer between matter and light, enabling the implementation of distributed quantum networking, has also been reported [13]. In networks of coupled quantum harmonic oscillators (HOs), on which we focus in the present work, the dynamics and manipulation of entanglement was analysed in [4, 7, 14]. We note that all the results mentioned above refer to ideal networks, where dissipative effects are absent, and thus the noise injection which introduces decoherence.

The need to store a quantum superposition against decoherence is necessarily a central issue within state transfer and protection in a realistic dissipative quantum network. Apart from the quest for computing the dynamical fidelity of a quantum superposition as it evolves through a dissipative quantum network, the search for a quantum storing device is of particular relevance for quantum information processing and future quantum communication networks [15]. In the present paper, we focus on the storage of quantum states against decoherence through their evolution in appropriate topologies of a network of dissipative HOs.

2. Network of dissipative harmonic oscillators

A given topology of a network composed by N HOs is defined by the way the oscillators are coupled together, the set of coupling strengths $\{\lambda_{mn}\}$ and their natural frequencies $\{\omega_m\}$. Here we assume the general scenario where each oscillator is coupled to its own reservoir, instead of the particular and rather unusual situation where the whole network is coupled to a common reservoir [8]. We start from a symmetric network, sketched in figure 1, where each oscillator is coupled to each other, apart from interacting with its own reservoir. Setting from here on that the indices m, m', n and n' run from 1 to N,

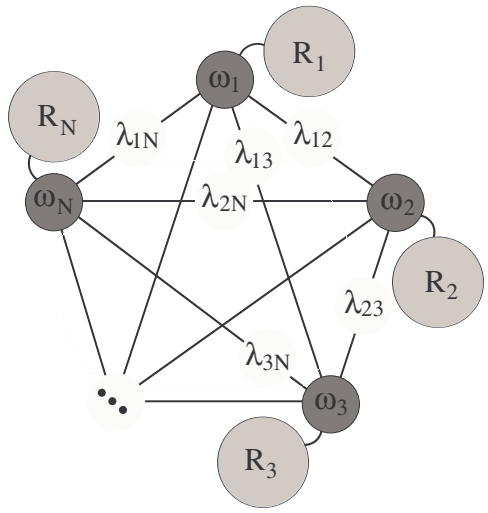

Figure 1. Sketch of a dissipative symmetric network.

the Hamiltonian $H = H_S + H_R + H_I$ modelling this network accounts for the N coupled oscillators,

$$H_S = \hbar \sum_m \left[\omega_m a_m^\dagger a_m + \frac{1}{2} \sum_{n(\neq m)} \lambda_{mn} \left(a_m^\dagger a_n + a_m a_n^\dagger \right) \right], \quad (1)$$

the N distinct reservoirs

$$H_R = \hbar \sum_m \sum_k \omega_{mk} b_{mk}^\dagger b_{mk}, \quad (2)$$

each one composed by an infinite set $\{k\}$ of modes, and the coupling between the HOs and their respective reservoirs,

$$H_I = \hbar \sum_m \sum_k V_{mk} \left(b_{mk}^\dagger a_m + b_{mk} a_m^\dagger \right). \quad (3)$$

In the above Hamiltonians, $a_m^\dagger$ (a_m) is the creation (annihilation) operator associated with the mth network oscillator ω_m which is coupled to the nth oscillator with strength λ_{mn} and to the mth reservoir with strength V_{mk}. The kth reservoir mode ω_{mk} is described by the creation (annihilation) operator $b_{mk}^\dagger$ (b_{mk}).

3. The master equation

To derive the master equation from Hamiltonian H, as done in [16], we first rewrite H_S in a matrix form $H_S = \hbar \sum_{m,n} a_m^\dagger \mathcal{H}_{mn} a_n$, with the elements given by

$$\mathcal{H}_{mn} = \omega_m \delta_{mn} + \lambda_{mn}(1 - \delta_{mn}). \quad (4)$$

The diagonalization of matrix $\mathcal{H}$ is thus performed through the transformation $A_m = \sum_n C_{mn} a_n$, where the coefficients of the mth line of matrix $\mathbf{C}$ define the eigenvectors associated with the eigenvalues ϖ_m of $\mathcal{H}$. With $\mathbf{C}$ being an orthogonal matrix, $\mathbf{C}^T = \mathbf{C}^{-1}$, the commutation relations $\left[A_m, A_n^\dagger \right] = \delta_{mn}$ and $[A_m, A_n] = 0$ follow, enabling the Hamiltonian H to be rewritten as $H = H_0 + V$, where

$$H_0 = \hbar \sum_m \left(\varpi_m A_m^\dagger A_m + \sum_k \omega_{mk} b_{mk}^\dagger b_{mk} \right) \quad (5a)$$

$$V = \hbar \sum_{m,n} \sum_k C_{nm} V_{mk} \left(b_{mk}^\dagger A_n + b_{mk} A_n^\dagger \right). \quad (5b)$$

With the diagonalized Hamiltonian H_0 we are ready to introduce the interaction picture, defined by the transformation $U(t) = \exp(-\mathrm{i}H_0 t/\hbar)$, in which $V_I(t) = \hbar \sum_{m,n} \left[\mathcal{O}_{mn}(t) A_n^\dagger + \mathcal{O}_{mn}^\dagger(t) A_n \right]$, and the bath operator $\mathcal{O}_{mn}(t) = C_{nm} \sum_k V_{mk} \exp[-\mathrm{i}(\omega_{mk} - \varpi_n)t] b_{mk}$. Assuming the interactions between the resonators and the reservoirs to be weak enough, we perform a second-order perturbation approximation followed by tracing out the reservoir degrees of freedom. We also assume a Markovian reservoir such that the density operator of the global system can be factorized as $\rho_{1\ldots N}(t) \otimes \rho_R(0)$. Defining the effective damping matrix whose elements are

$$\Gamma_{mn} = N \sum_{n'} C_{n'm} \gamma_m(\varpi_{n'}) C_{n'n}, \quad (6)$$

where $\gamma_m(\varpi_{n'})$ is the damping rate of the mth oscillator around the normal modes $\varpi_{n'}$, the master equation for a reservoir at 0 K simplifies to the generalized Lindblad form

$$\frac{\mathrm{d}}{\mathrm{d}t} \rho_S(t) = \frac{\mathrm{i}}{\hbar} [\rho_S(t), H_0] + \sum_{m,n} \mathcal{L}_{mn} \rho_S(t), \quad (7)$$

where

$$\mathcal{L}_{mn} \rho_S(t) = \sum_{m,n} \frac{\Gamma_{mn}}{2} \left(\left[a_n \rho_S(t), a_m^\dagger \right] + \left[a_m, \rho_S(t) a_n^\dagger \right] \right) \quad (8)$$

are the Liouville operators accounting for the direct $(m = n)$ and indirect $(m \neq n)$ dissipative channels. Through the direct channels the oscillators lose excitation to their own reservoirs, whereas through the indirect channels they lose excitation to all the other reservoirs but not to their own. We observe that for Markovian white noise reservoirs, $\gamma_m(\varpi_n) = \gamma_m$, equation (6) reduces to $\Gamma_{mn} = N \gamma_m \delta_{mn}$, and the indirect channels become null.

4. The Glauber–Sudarshan *P*-function

The evolution equation for the Glauber–Sudarshan P-function, derived from the master equation (7), is given by

$$\frac{\mathrm{d}}{\mathrm{d}t} P(\{\eta_m\}, t) = \sum_m \left(\frac{\Gamma_{mm}}{2} + \sum_n \mathcal{H}_{mn}^D \eta_n \frac{\partial}{\partial \eta_m} + \text{c.c.} \right) P(\{\eta_m\}, t), \quad (9)$$

where, generalizing matrix $\mathcal{H}$ (4), we have defined its dissipative counterpart $\mathcal{H}^D$, with the elements

$$\mathcal{H}_{mn}^D = \mathrm{i}\mathcal{H}_{mn} + \Gamma_{mn}/2. \quad (10)$$

The solution to equation (9) factorizes as [16]

$$P(\{\eta_m\}, t) = \exp\left(\sum_m \Gamma_{mm} t \right) [P(\{\eta_m\}, t = 0)|_{\{\eta_m\} \to \{\eta_m(t)\}},$$

where $\eta_m(t) = \sum_{m',n} D_{mn} \exp(\Omega_n t) D_{nm'}^{-1} \eta_{m'}$ and the elements of the mth column of matrix $\mathbf{D}$ define the mth eigenvector associated with the eigenvalue Ω_m of matrix $\mathcal{H}^D$. Having the P-function at time $t = 0$, we immediately obtain it at any other

time by substituting the initial set $\{\eta_n\}$ with the evolved one $\{\eta_n(t)\}$.

After introducing the matrix $\mathcal{H}^D$ we are in the position to build up whichever the topology of the network. The general symmetric dissipative topology $\mathcal{H}^D_{sym}$, from which all other are derived, is sketched in figure 1. From equations (6) and (10), we verify that the matrix $\mathcal{H}^D_{sym}$ describing such a topology is given by

$$\mathcal{H}^D_{sym} = \frac{1}{2}\begin{pmatrix} \Gamma_{11} & \Gamma_{12} & \cdots & \Gamma_{1N} \\ \Gamma_{21} & \Gamma_{22} & \cdots & \Gamma_{2N} \\ \vdots & \vdots & \ddots & \vdots \\ \Gamma_{N1} & \Gamma_{N2} & \cdots & \Gamma_{NN} \end{pmatrix} + \mathrm{i}\begin{pmatrix} \omega_1 & \lambda_{12} & \cdots & \lambda_{1N} \\ \lambda_{12} & \omega_2 & \cdots & \lambda_{2N} \\ \vdots & \vdots & \ddots & \vdots \\ \lambda_{1N} & \lambda_{2N} & \cdots & \omega_N \end{pmatrix}, \tag{11}$$

where the first matrix describes the nondissipative network, and the second accounts for the dissipation.

5. The density operator and decoherence time

Let us consider that the initial pure state of the network is given by a general superposition whose density operator reads $\rho(0) = \mathcal{N}^2\sum_{r,s} c_r c_s^* \big|\{\beta_m^r\}\big\rangle\big\langle\{\beta_m^s\}\big|$, where $\mathcal{N}$ is the normalization factor and c_r is the probability amplitudes of the direct product of coherent states $\big|\{\beta_m^r\}\big\rangle = \bigotimes_m \big|\beta_m^r\big\rangle$. After some algebra we verify that $\rho(0)$ evolves to the reduced network density operator

$$\rho_S(t) = \mathcal{N}^2 \sum_{r,s} c_r c_s^* \frac{\big\langle\{\beta_m^s\}\big|\{\beta_m^r\}\big\rangle}{\big\langle\{\zeta_m^s(t)\}\big|\{\zeta_m^r(t)\}\big\rangle} \big|\{\zeta_m^r(t)\}\big\rangle\big\langle\{\zeta_m^s(t)\}\big|, \tag{12}$$

where the excitation of the mth oscillator is given by $\zeta_m^r(t) = \sum_n \Theta_{mn}(t)\beta_n^r$, with the time-dependent matrix elements $\Theta_{mn}(t) = \sum_{m'} D_{mm'}\exp(-\Omega_{m'}t)D^{-1}_{m'n}$.

From the general form given in $\rho(0)$, we choose the particular initial state of the network $|\Psi(0)\rangle = \mathcal{N}(|\alpha\rangle + |-\alpha\rangle)_1 \otimes |\{\xi_\ell\}\rangle$, where a superposition of coherent states prepared in oscillator 1 factorizes from a product of coherent (or vacuum) states ξ prepared in the remaining oscillators, with ℓ running from 2 to N from here on. Evidently, the state prepared in HO 1 is the one to be protected through its evolution across an appropriate topology of the network. For the state of interest $|\Psi(0)\rangle$, expression (12) simplifies to

$$\rho_S(t) = \mathcal{N}^2 \sum_{r,s} c_r c_s^* \exp\{-[2|\alpha|^2\mathcal{F}(t) - i\mathcal{G}_r(t)](1-\delta_{rs})\} \times \big|\{\zeta_m^r(t)\}\big\rangle\big\langle\{\zeta_m^s(t)\}\big|, \tag{13}$$

where $\mathcal{F}(t) = 1 - \sum_m |\Theta_{m1}(t)|^2$ and $\mathcal{G}_r(t) = 2\sum_{m,n} \mathrm{Im}\big[\xi^*\beta_1^r\Theta_{m1}(t)\Theta^*_{mn}(t)\big]$. Regarding the decoherence time of the superposition $\mathcal{N}(|\alpha\rangle + |-\alpha\rangle)_1$, it can be immediately estimated from the exponential decay $\exp[-2|\alpha|^2\mathcal{F}(t)]$ of the off-diagonal terms of the density operator (13) as

$$\tau_D^{-1} = \lim_{t\to 0}[2|\alpha|^2\mathcal{F}(t)/t]. \tag{14}$$

We note that for an isolated dissipative HO, the decoherence time of the superposition $\mathcal{N}(|\alpha\rangle + |-\alpha\rangle)_1$, following from $\mathcal{F}(t) = 1 - \mathrm{e}^{-\gamma t}$, equals to $(2|\alpha|^2\gamma)^{-1}$.

6. The memory device

On building up the memory device for the superposition $\mathcal{N}(|\alpha\rangle + |-\alpha\rangle)_1$ prepared in the HO 1, we assume that the decay rate of this oscillator is γ, with all the other decay rates being $\tilde{\gamma} \ll \gamma$. In current cavity QED technology, we can assign the value $\gamma \approx 10^3\ \mathrm{s}^{-1}$ for a high-Q open cavity [17], playing the role of the HO 1, where the state can be prepared and subsequently read out through atom–field interactions. In this context, highest-Q closed cavities, all with $\tilde{\gamma} \approx 1\ \mathrm{s}^{-1}$ [18], play the role of the remaining storage HOs. We thus consider the open cavity to manipulate the field state through atom–field interaction, while the closed cavities are only assigned for the storing process. Before analysing numerically large networks, we first address the cases $N = 2, 3$ and 4 under the regime of parameters $\{\gamma_{m'}\} \ll \{\lambda_{mn}\} \ll \{\omega_{n'}\}$ and Markovian white noise reservoirs, which allows for analytical results.

(i) *The case* $N = 2$. Even such a minimal network defining a trivial topology operates as a memory device. In fact, the obtained $\mathcal{F}^{(N=2)}(t) = 1 - \mathrm{e}^{-(\gamma+\tilde{\gamma})t/2}$ prompts the decoherence time

$$\tau_D^{(N=2)} = \frac{1}{2|\alpha|^2}\frac{2}{\gamma+\tilde{\gamma}} \simeq 2\frac{1}{2|\alpha|^2\gamma}, \tag{15}$$

which is about twice the value assigned for a dissipative HO 1 uncoupled from the network [7].

(ii) *The case* $N = 3$. From a symmetric network with $N = 3$, we obtain, up to terms of the orders $\mathcal{O}(\gamma/\{\lambda_{mn}\})$ and $\mathcal{O}(\tilde{\gamma}/\{\lambda_{mn}\})$, the function

$$\mathcal{F}^{(N=3)}(t) \approx \left[\left(1 + \frac{\big(\lambda_{12}^2 + \lambda_{13}^2 - 2\lambda_{23}^2\big)^2\Lambda^2}{18(\Lambda^6 - \Delta^6)}\right)\frac{\gamma-\tilde{\gamma}}{3} + \tilde{\gamma}\right]t, \tag{16}$$

where $\Lambda^2 = \big(\lambda_{12}^2 + \lambda_{13}^2 + \lambda_{23}^2\big)/3$ and $\Delta^3 = \lambda_{12}\lambda_{13}\lambda_{23}$. In this case, as in any other where $N \geqslant 3$, the appropriate topologies for optimal memory devices follows automatically from the maximization of the decoherence time (minimization of $\mathcal{F}(t)$). Such a maximization procedure imposes the relation $\lambda_{23}^2 = \big(\lambda_{12}^2 + \lambda_{13}^2\big)/2$, with the additional restriction $\lambda_{12} \neq \lambda_{13}$, which results in two possible topologies: a circular network (see figure 2) with all the couplings λ_{mn} being distinct and nonzero, and a linear network with $\lambda_{13} = 0$. In both cases the decoherence time of the superposition $\mathcal{N}(|\alpha\rangle + |-\alpha\rangle)_1$ is given by

$$\tau_D^{(N=3)} = \frac{1}{2|\alpha|^2}\frac{3}{\gamma+2\tilde{\gamma}} \simeq 3\frac{1}{2|\alpha|^2\gamma}, \tag{17}$$

which is three times larger than the value assigned for an isolated dissipative HO 1.

(iii) *The case* $N = 4$. We refrain from presenting here the long expression derived for $\mathcal{F}^{(N=4)}(t)$, whose minimization results on the condition $\lambda_{12}^2 + \lambda_{13}^2 = \lambda_{24}^2 + \lambda_{34}^2$ with $\lambda_{14} = \lambda_{23} = 0$ (which is entirely equivalent to $\lambda_{13}^2 + \lambda_{14}^2 = \lambda_{23}^2 + \lambda_{24}^2$ with

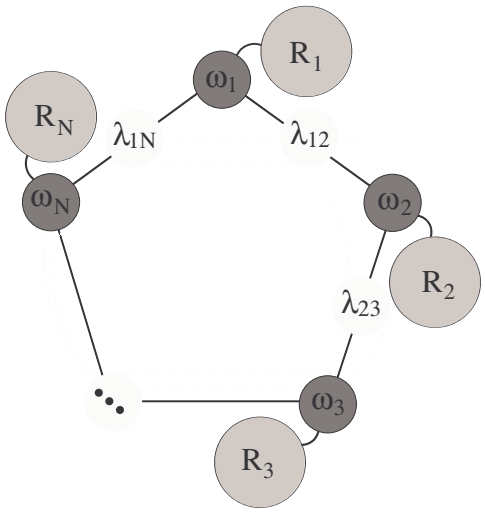

Figure 2. Sketch of a dissipative circular network.

$\lambda_{12} = \lambda_{34} = 0$ and $\lambda_{12}^2 + \lambda_{14}^2 = \lambda_{23}^2 + \lambda_{34}^2$ with $\lambda_{13} = \lambda_{24} = 0$). As in the case $N = 3$, this condition results in two optimal memory devices builded up from a circular or a linear network, both given a decoherence time four times larger than that for an isolated dissipative HO 1,

$$\tau_D^{(N=4)} = \frac{1}{2|\alpha|^2}\frac{4}{\gamma + 3\tilde{\gamma}} \simeq 4\frac{1}{2|\alpha|^2\gamma}. \tag{18}$$

From expressions (15)–(18), and an appropriate choice of the coupling strengths λ_{mn} defining the circular and linear topologies of a network with N HOs, we are encouraged to propose the conjecture that the decoherence time for any N can be expressed as

$$\tau_D^{(N)} = \frac{1}{2|\alpha|^2}\frac{N}{\gamma + (N-1)\tilde{\gamma}}. \tag{19}$$

This conjecture is corroborated by numerical calculation, presented in figure 3, apart from an additional heuristic argument discussed below. We also infer that the coupling strengths λ_{mn} must satisfy the constraint

$$(N-2)\left(\lambda_{12}^2 + \lambda_{1N}^2\right) = 2\sum_{m=2}^{N-1}\lambda_{m,m+1}^2, \tag{20}$$

with all the other couplings set equal to zero. This constraint and $\tau_D^{(N)}$ will be numerically verified below. Both circular and linear topologies composing a memory device with N HOs are described by the sum of matrices,

$$\mathcal{H}^D_{\binom{\text{cir}}{\text{lin}}} = i\begin{pmatrix} \omega_1 & \lambda_{12} & 0 & \cdots & \mathcal{H}_{1N}^{\binom{\text{cir}}{\text{lin}}} \\ \lambda_{12} & \omega_2 & \lambda_{23} & \cdots & 0 \\ 0 & \lambda_{23} & \omega_3 & \ddots & 0 \\ \vdots & \vdots & \ddots & \ddots & \vdots \\ \mathcal{H}_{1N}^{\binom{\text{cir}}{\text{lin}}} & 0 & 0 & \cdots & \omega_N \end{pmatrix} + \frac{1}{2}\begin{pmatrix} \Gamma_{11} & \Gamma_{12} & \cdots & \Gamma_{1N} \\ \Gamma_{21} & \Gamma_{22} & \cdots & \Gamma_{2N} \\ \vdots & \vdots & \ddots & \vdots \\ \Gamma_{N1} & \Gamma_{N2} & \cdots & \Gamma_{NN} \end{pmatrix}, \tag{21}$$

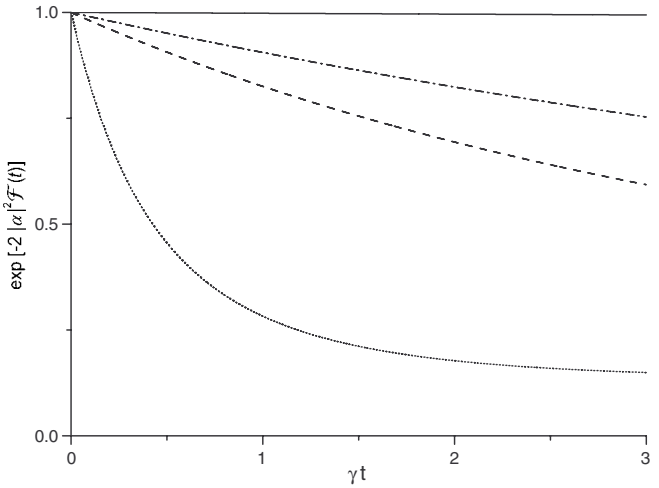

Figure 3. Plot of the numerically computed exponential decay $\exp[-2|\alpha|^2\mathcal{F}(t)]$ for $N = 10$ and $N = 20$ (dashed and dashed-dotted), for comparison and validation of the inferred analytical result in equation (19). The solid and dotted curves give the less and more pronounced decays coming from the analytical results $\mathcal{F}(t) = 1 - \mathrm{e}^{-\tilde{\gamma}t}$ (when $\gamma \ll N\tilde{\gamma}$) and $\mathcal{F}(t) = 1 - \mathrm{e}^{-\gamma t}$ (when the dissipative HO 1 is isolated), respectively.

where $\mathcal{H}^D_{\text{cir}}$ and $\mathcal{H}^D_{\text{lin}}$ differ from each other only by the elements $\mathcal{H}^{\text{cir}}_{1N} = \lambda_{1N}$ and $\mathcal{H}^{\text{lin}}_{1N} = 0$. In figure 2 we sketch the circular network, noting that the linear one follows directly by switching off the coupling λ_{1N}.

We observe from expression (19) that, when $\gamma \gg N\tilde{\gamma}$, the decoherence time of the superposition $\mathcal{N}(|\alpha\rangle + |-\alpha\rangle)_1$ prepared in the HO 1 becomes, remarkably, as large as the number of HOs in the network, i.e., $\tau_D^{(N)} = N/(2|\alpha|^2\gamma)$. Even better, when $\gamma \ll N\tilde{\gamma}$, the decoherence time becomes proportional to the much higher relaxation time $\tilde{\gamma}^{-1}$, i.e., $\tau_D^{(N)} = (2|\alpha|^2\tilde{\gamma})^{-1}$. We stress that, apart from both optimum topologies which maximize the decoherence time, as given by equation (19), all the other possible topologies (with whichever the set of coupling parameters $\{\lambda_{mn}\}$) also works as a memory device, increasing the decoherence time computed when an isolated dissipative HO is considered.

Next, we confirm the validity of the inferred equation (19) by plotting in figure 3 the numerically computed exponential decay $\exp[-2|\alpha|^2\mathcal{F}(t)]$, versus γt, for whichever the circular or linear topology of networks with $N > 4$ HOs. For $\alpha = 1$, $\tilde{\gamma}/\gamma = 10^{-3}$, and $\lambda_{12}/\sqrt{2}\gamma = \lambda_{23}/\gamma = \cdots = \lambda_{N-1,N}/\gamma = 10^3/\sqrt{2}$, the dashed and dashed-dotted curves correspond to $N = 10$ and 20, respectively. These numerical curves are compared with those obtained analytically from the decoherence time (19), by substituting $\mathcal{F}(t) = 1 - \exp\{-[\gamma + (N-1)\tilde{\gamma}]t/N\}$ into $\exp[-2|\alpha|^2\mathcal{F}(t)]$. The inferred analytical results fit exactly the numerical calculations. We also plot in figure 3, for comparison with the exponential decays for $N = 10$ and 20, the solid and dotted curves given the less and more pronounced decays coming from the analytical results $\mathcal{F}(t) = 1 - \mathrm{e}^{-\tilde{\gamma}t}$ (when$\gamma \ll N\tilde{\gamma}$) and $\mathcal{F}(t) = 1 - \mathrm{e}^{-\gamma t}$ (when the dissipative HO 1 is isolated), respectively.

A consistent heuristic argument may be given to support our conclusion that the optimal topologies are indeed the

circular and the linear one for any number of oscillators. In fact, the most general expression for the decoherence time of the superposition state $\mathcal{N}(|\alpha\rangle + |-\alpha\rangle)$—following from the relation $\tau_D^{-1} = \lim_{t\to 0}[2|\alpha|^2\mathcal{F}(t)/t]$ estimated from the exponential decay $\exp[-2|\alpha|^2\mathcal{F}(t)]$ of the off-diagonal terms of the density operator (13)—is given by

$$\tau_D = \frac{f}{2|\alpha|^2(g\gamma + h\widetilde{\gamma})} = \frac{\tilde{f}}{2|\alpha|^2(\gamma + \tilde{h}\widetilde{\gamma})}, \tag{22}$$

where f, g and h can be general dimensionless functions of N, $\{\lambda_{mn}\}$ and $\{\omega_n\}$, with $\tilde{f} = f/g$ and $\tilde{h} = h/g$. In fact, the above expression is the more general form since both decay rates γ and $\widetilde{\gamma}$ must appear in the denominator of the expression considered up to order γt ($\widetilde{\gamma}t$). We note that, to first order in γt, the time-dependent function $\mathcal{F}(t) = 1 - \sum_m |\Theta_{m1}(t)|^2$ in the exponential decay $\exp[-2|\alpha|^2\mathcal{F}(t)]$ is of the form $(g\gamma + h\widetilde{\gamma})t/f$. Now, considering the particular case $\gamma = \widetilde{\gamma}$, it can be straightforwardly verified that the decoherence time of the superposition $\mathcal{N}(|\alpha\rangle + |-\alpha\rangle)$ is given by the standard result $(2|\alpha|^2\gamma)^{-1}$ of an isolated dissipative harmonic oscillator, leading to the additional requirement $\tilde{f} = 1 + \tilde{h}$. Analysing this requirement in the light of our analytical expressions $\tau_D^{(N=3)}$ and $\tau_D^{(N=4)}$ (apart from the inferred one $\tau_D^{(N)}$), we set the optimal value $\tilde{f} = N$ with $\tilde{h} = N - 1$. The above reasonable construction gave us the confidence to conclude that we have inferred the optimum topologies for a network with any number N of coupled harmonic oscillators.

7. Retrieving the stored state

For the specific topologies derived above to work as a genuine memory device, we must be able to retrieve and make available back into the HO 1, the information content of the evolved initial superposition $\mathcal{N}(|\alpha\rangle + |-\alpha\rangle)_1$. To show that such an information content recurs many times back into the HO 1, before accumulating a significant reduction of its fidelity due to decoherence, we derive the recurrence time τ_R from the maximum of the recurrence probability (or fidelity)

$$\begin{aligned}\mathcal{P}_R(t) &= \mathrm{Tr}[\rho_1(t)\rho_1(0)] \\ &= \mathcal{N}^4 \sum_{r,s,r',s'} \frac{\langle\beta_1^s|\beta_1^r\rangle}{\langle\zeta_1^s(t)|\zeta_1^r(t)\rangle}\langle\zeta_1^s(t)|\beta_1^{r'}\rangle\langle\beta_1^{s'}|\zeta_1^r(t)\rangle,\end{aligned} \tag{23}$$

where $\rho_1(t) = \mathrm{Tr}_{2\cdots N}\rho_S(t)$ [7]. Evidently, for the case of ideal cavities ($\gamma = \widetilde{\gamma} = 0$), the maximum of the recurrence probability equal unity. For the case $N = 3$ with $\omega_m = \omega$, we obtain

$$\Lambda\tau_R = j\pi, \tag{24}$$

where the allowed values for the integers j, k and l, follow when both equalities

$$j = \frac{k}{\sqrt{3}}\cot(\theta/3) = l\frac{2\Lambda}{\omega}\cos(\theta/3) \tag{25}$$

are simultaneously satisfied, under the condition that j and k must be both even or odd, with $\theta = \arctan\sqrt{(\Lambda/\Delta)^6 - 1}$. For a linear network with $N = 3$, where $\Delta = \lambda_{13} = 0$ and consequently $\theta = \pi/2$, the choice $\Lambda/\omega = 1/\sqrt{3}$ also results in the recurrence time given by equation (24), but $\Lambda\tau_R = j\pi$ ($j = 1, 2, 3, \ldots$), which goes proportional to the timescale Λ^{-1}, defined by the coupling strength, which is evidently expected to be significantly smaller than both the shortest decoherence timescale γ^{-1} and, consequently, of longest $\tilde{\gamma}^{-1}$. For the case where $\Lambda/\omega \ll 1$ (expected to be applicable for cavity quantum electrodynamics), it can be verified that τ_R is obtained when only the first equality in equation (25) is verified.

For $N = 2$, the recurrence time follows directly from equation (25) by turning off the couplings λ_{13} and λ_{23}. In this case, where $\theta = \pi/2$, the first equality in equation (25) reduces to a single expression and, consequently, the recurrence time is found when only a single equality is satisfied, making it shorter than in the case $N = 3$. Conversely, for $N = 4$ the recurrence time is found when the three equalities are simultaneously satisfied, thus making τ_R longer than in the case $N = 3$. As expected, the larger the network the longer the recurrence time. However, it can be verified that the longer recurrence times established for large networks are still considerably smaller than the associated decoherence time. In fact, as verified in [7], for the simplest case where all the couplings have the same strength, the recurrence time for large values of N goes as $N\Lambda^{-1}$. When $\Lambda \gg \gamma$, such a timescale $N\Lambda^{-1}$ is expected to be easily surpassed by both decoherence timescales, γ^{-1} for the case of small N ($\gamma \gg N\tilde{\gamma}$) and, even more easily, $\tilde{\gamma}^{-1}$ for the case of large N ($\gamma \ll N\tilde{\gamma}$). When considering different coupling strengths, as envisaged for the construction of our memory devices, the magnitude of τ_R does not differ greatly from $N\Lambda^{-1}$, as long as a circular or a linear topology is considered. In this regard, we note from the general condition (20) for maximizing the decoherence time (19), that special sets $\{\lambda_{mn}\}$ can be engineered, leading to the desired recurrence times.

To illustrate the recurrence of a superposition, assumed to be a 'Schrödinger cat'-like state $\mathcal{N}(|\alpha\rangle + |-\alpha\rangle)$, back into the HO 1, we plot in figure 4 the probability of recurrence $\mathcal{P}_R(t)$ (solid line) and the inferred optimized coherence decay $\exp\{-2|\alpha|^2[1 - \mathrm{e}^{-[\gamma+(N-1)\tilde{\gamma}]t/N}]\}$ (thick solid line), versus γt, assuming that all the storage HOs are initially in the vacuum state. In figures 4(a)–(c) we contemplate the cases $N = 3, 4$ and 6, respectively, considering a degenerate circular network with the ratios $\omega/\gamma = 10^5, \lambda/\gamma = 10^3, \widetilde{\gamma}/\gamma = 10^{-3}$ and $|\alpha|^2 = 10$. We observe that, apart from recurring many times back into the HO 1 within the decoherence time (under the reasonable assumption that $\lambda/\gamma \gg 1$), the probability of recurrence decays at a slower rate compared with the coherence decay. Such a high amplitude for the probability of recurrence, overcoming even the optimized coherence decay, is an additional attractive feature of the present storing device. The shaded regions between two consecutive recurrences follow from the strong oscillations of the probability $\mathcal{P}_R(t)$ even under the modest ratio $\omega/\gamma = 10^5$. We also observe that the recurrence time increases with the number of the storage HOs. However, as seen from figure 4(d), where we have considered the same parameters as in figure 4(c), but changing the ratio λ/γ from 10^3 to 2×10^3, the increase of the coupling strength between the HOs leads to the decrease of the recurrence time. We also note that the curves in figure 4

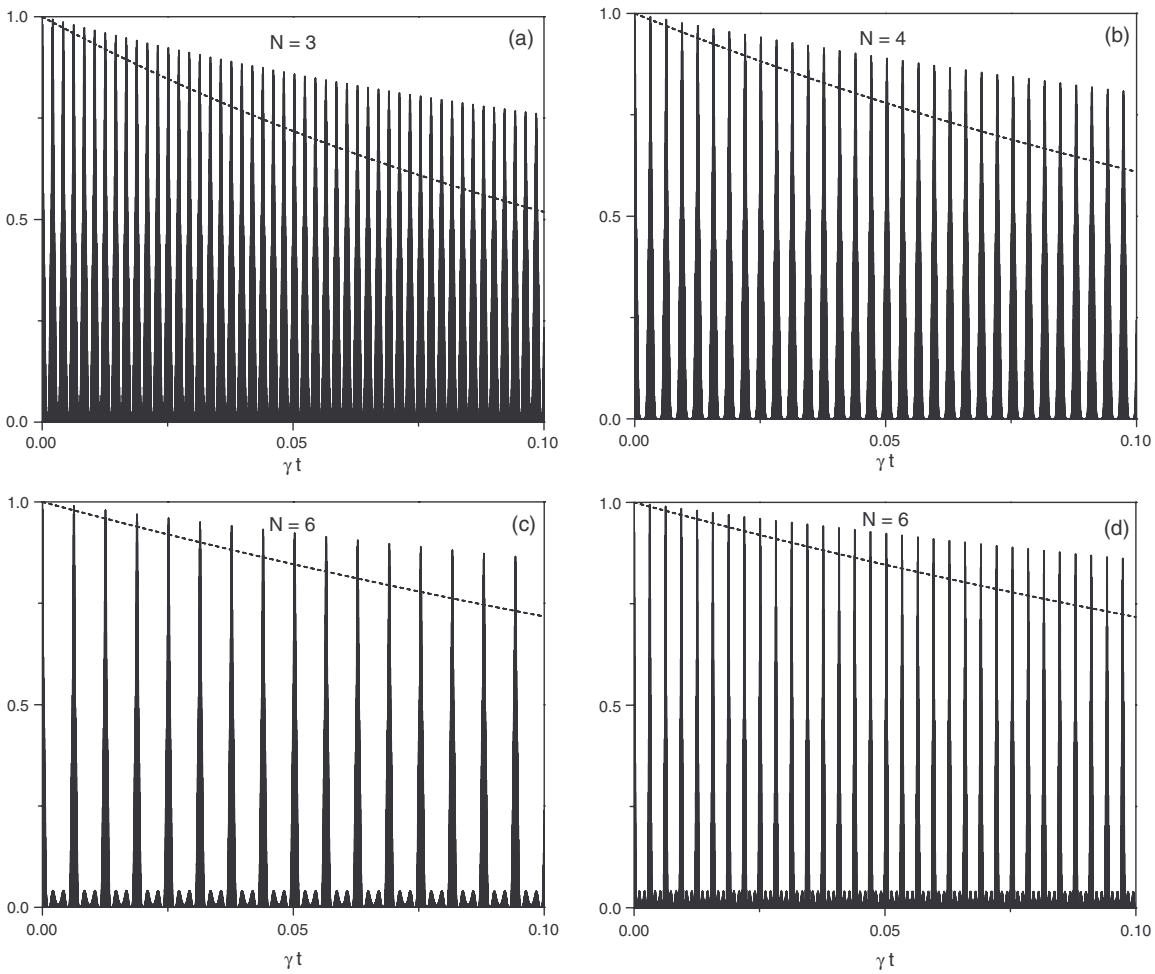

Figure 4. Plot the probability of recurrence $\mathcal{P}_R(t)$ (solid line) and the coherence decay $\exp\{-2|\alpha|^2[1-\mathrm{e}^{-[\gamma+(N-1)\tilde{\gamma}]t/N}]\}$ (thick solid line), versus γt, for the cases (a) $N=3$, (b) $N=4$ and (c) $N=6$ setting $\omega/\gamma=10^5$, $\lambda/\gamma=10^3$, $\tilde{\gamma}/\gamma=10^{-3}$ and $|\alpha|^2=10$. In figure 4(d) we set the same parameters as in figure 4(c), but changing $\lambda/\gamma=10^3$ to 2×10^3.

follow from the regime where $\gamma \gg N\tilde{\gamma}$; otherwise, for $\gamma \ll N\tilde{\gamma}$, the pattern of the probability of recurrence remains the same as that for $\gamma \gg N\tilde{\gamma}$, with the decay of the probability of recurrence also exceeding the coherence decay given by $\exp[-2|\alpha|^2(1-\mathrm{e}^{-\tilde{\gamma}t})]$.

To demonstrate that the decay of decoherence occurs at a higher rate than that of the probability of recurrence for any N, in figure 5 we plot the difference between the envelope function of the probability of recurrence $\mathbb{E}[\mathcal{P}_R(t)]$ and the coherence decay, defined as $\mathcal{D}(t)=\mathbb{E}[\mathcal{P}_R(t)]-\exp\{-2|\alpha|^2[1-\mathrm{e}^{-[\gamma+(N-1)\tilde{\gamma}]t/N}]\}$, against the scaled $\gamma t/N$. We consider the cases $N=2$ (thick solid line), 3 (dotted), 4 (dashed line), 5 (dashed-dotted) and 6 (solid line), setting again the ratios $\omega/\gamma=10^5, \lambda/\gamma=10^3, \tilde{\gamma}/\gamma=10^{-3}$ and $|\alpha|^2=10$. We observe that the decay of function $\mathcal{D}(t)$—after reaching the maximum around the decoherence time indicated by the vertical dotted line at $\gamma t/N=0.1$—slows down with the increase of either the even $N=2,4$ and 6 or the odd $N=3,5$. The fact that the difference $\mathcal{D}(t)$ is practically the same for any N until the decoherence time has elapsed, ensures that our device is suitable for use as a quantum memory.

Next, we demonstrate analytically that the envelope function of the probability of recurrence, $\mathbb{E}[\mathcal{P}_R(t)]$, is always higher than the coherence decay. To this end, we note that the probability of recurrence satisfies the relation

$$\begin{aligned}\mathcal{P}_R(t) &= \mathrm{Tr}[\rho_1(t)\rho_1(0)] \geqslant \mathrm{Tr}[\rho_S(t)\rho_S(0)] \\ &= \mathcal{N}^4 \sum_{r,s,r',s'} \frac{\langle\{\beta_m^s\}|\{\beta_m^r\}\rangle}{\langle\{\zeta_m^s(t)\}|\{\zeta_m^r(t)\}\rangle}\langle\{\zeta_m^s(t)\}|\{\beta_m^{r'}\}\rangle \\ &\quad\times\langle\{\beta_m^{s'}\}|\{\zeta_m^r(t)\}\rangle, \end{aligned} \tag{26}$$

stressing that the probability for the initial 'Schrödinger cat'-like state $\mathcal{N}(|\alpha\rangle+|-\alpha\rangle)$ to recur to the HO 1 is, evidently, lower bounded by the probability for the initial state of the whole network (the HO 1 included) to recur. While the ratio $\langle\{\beta_m^s\}|\{\beta_m^r\}\rangle/\langle\{\zeta_m^s(t)\}|\{\zeta_m^r(t)\}\rangle$, appearing in equation (12), gives the coherence decay $\exp\{-2|\alpha|^2[1-\mathrm{e}^{-[\gamma+(N-1)\tilde{\gamma}]t/N}]\}$, the product between this ratio and the factor $\langle\{\zeta_m^s(t)\}|\{\beta_m^{r'}\}\rangle\langle\{\beta_m^{s'}\}|\{\zeta_m^r(t)\}\rangle$, as seen from equation (26), gives the upper bound for the envelope decay. When considering that a 'Schrödinger cat'-like state $\mathcal{N}(|\alpha\rangle+|-\alpha\rangle)$ is prepared in the HO1 while all the storage HOs are initially in the vacuum state, the ratio $\langle\{\beta_m^s\}|\{\beta_m^r\}\rangle/\langle\{\zeta_m^s(t)\}|\{\zeta_m^r(t)\}\rangle$ decays from 1 to $\exp(-2|\alpha|^2)$ while the factor $\langle\{\zeta_m^s(t)\}|\{\beta_m^{r'}\}\rangle\langle\{\beta_m^{s'}\}|\{\zeta_m^r(t)\}\rangle$ increases from $\exp(-4|\alpha|^2)$ to $\exp(-|\alpha|^2)$. This simple analysis explains why

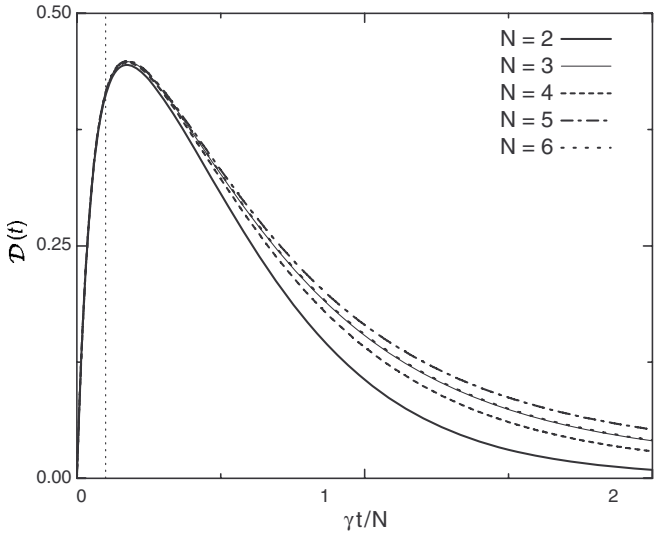

Figure 5. Plot of the difference $\mathcal{D}(t) = \mathbb{E}[\mathcal{P}_R(t)] - \exp\{-2|\alpha|^2[1 - e^{-[\gamma+(N-1)\tilde{\gamma}]t/N}]\}$ against the normalized $\gamma t/N$, for the cases $N = 2$ (thick solid line), 3 (dotted), 4 (dashed line), 5 (dashed-dotted) and 6 (solid line), considering the ratios $\omega/\gamma = 10^5$, $\lambda/\gamma = 10^3$, $\widetilde{\gamma}/\gamma = 10^{-3}$ and $|\alpha|^2 = 10$.

the difference $D(t)$ is always a positive quantity as shown in figure 5.

8. Concluding remarks

We have shown how to protect a superposition prepared in a single HO with decay rate γ by coupling it to a circular or linear chain of HOs all with the same decay rate $\tilde{\gamma} \ll \gamma$. Whereas the memory devices presented in the literature rely entirely on the significantly large decay rate of the storage system, where a stationary state is guarded from the environment, the dynamical device presented here combines both the large decay rate of the storage HOs and specific evolutions of the state to be protected through the network. We have illustrated the application of our memory device in the domain of cavity QED because the manipulation of a cavity-field state must be accomplished (through atom–field interactions) in an open cavity exhibiting a large decay rate compared to a closed one. These latter higher-Q cavities are then used to store the superposition states which are retrieved in the open cavity where they were prepared. Therefore, our scheme applies whenever the preparation of the state to be protected demands 'open' systems with higher-decay rates than 'closed' storage systems not suitable to state manipulation. As a memory device must certainly play a major role in the development and prospects of quantum information theory, we believe that the reasoning presented in this paper can be useful in the domain of quantum information theory. Although the application of the present storing device for recent potential networks [19, 20] seems not to be automatic, the reasoning here presented, leading to equation (19), can guide further investigations on decoherence control in a quantum network.

Acknowledgments

We wish to express thanks for the support from FAPESP and CNPq, Brazilian agencies.

References

[1] Mandel O, Greiner M, Widera A, Rom T, Hänsch T W and Bloch I 2003 *Phys. Rev. Lett.* **91** 010407
Feder D L 2006 *Phys. Rev. Lett.* **97** 180502
[2] Polkovnikov A 2003 *Phys. Rev.* A **68** 033609
Burgarth D and Bose S 2005 *Phys. Rev.* A **71** 052315
[3] Christaldl M, Datta N, Ekert A and Landahl A J 2004 *Phys. Rev. Lett.* **92** 187902
[4] Plenio M B, Hartley J and Eisert J 2004 *New J. Phys.* **6**
[5] Chou C W, Laurat J and Deng H *et al* 2007 *Science* **316** 1316
[6] Raimond J M, Brune M and Haroche S 1997 *Phys. Rev. Lett.* **79** 1964
[7] Ponte M A de, de Oliveira M C and Moussa M H Y 2005 *Ann. Phys., NY* **317** 72
de Ponte M A, de Oliveira M C and Moussa M H Y 2004 *Phys. Rev.* A **70** 022324
de Ponte M A, de Oliveira M C and Moussa M H Y 2004 *Phys. Rev.* A **70** 022325
[8] de Ponte M A, Mizrahi S S and Moussa M H Y 2007 *Ann. Phys., NY* **322** 2077
[9] Osterloh A, Amico L and Falci G *et al* 2002 *Nature* **416** 6881
[10] Lambert N, Emary C and Brandes T 2004 *Phys. Rev. Lett.* **92** 073602
[11] Dunning C, Links J and Zhou H Q 2005 *Phys. Rev. Lett.* **94** 227002
[12] Chiaverini J, Leibfried D and Schaetz T *et al* 2004 *Nature* **432**
Kuzmich A, Bowen W P and Boozer A D *et al* 2003 *Nature* **423**
Cirac J L and Zoller P 2000 *Nature* **404** 579
[13] Matsukevich D N and Kuzmich A 2004 *Science* **306**
[14] de Oliveira M C, Mizrahi S S and Dodonov V V 1999 *J. Opt.* B **1** 610
[15] Rosenfeld W, Berner S and Volz J *et al* 2007 *Phys. Rev. Lett.* **98** 050504
[16] de Ponte M A, Mizrahi S S and Moussa M H Y 2007 *Phys. Rev.* A **76** 032101
[17] Raimond J M, Brune M and Haroche S 2001 *Rev. Mod. Phys.* **73** 565
[18] Brattke S, Varcoe B T H and Walther H 2001 *Phys. Rev. Lett.* **86** 3534
[19] Blais A, Huang R-S and Wallraff A *et al* 2004 *Phys. Rev.* A **69** 062320
Blais A, Gambetta J and Wallraff A *et al* 2007 *Phys. Rev.* A **75** 032329
[20] Painter O *et al* 1999 *Science* **284** 1819
Strauf S *et al* 2006 *Phys. Rev. Lett.* **96** 127404
Akahane Y, Asano T, Song B S and Noda S 2003 *Nature* **425** 944